Comparison of remote sensing based GPP models at an alpine meadow site

WANG Xufeng[1,2], MA Mingguo[1], LI Xin[1], SONG Yi[1,2], TAN Junlei[1], HUANG Guanghui[1], YU Wenping[1,2]

1. *Cold and Arid Regions Remote Sensing Observation System Experiment Station*, *Cold and Arid Regions Environmental and Engineering Research Institute*, *Chinese Academy of Sciences*, *CAS*, *Lanzhou* 730000, *China*;
2. *Graduate University of Chinese Academy of Sciences*, *Beijing* 100049, *China*

Abstract: Development of remote sensing makes it possible to estimate Gross Primary Productivity (GPP) regionally. In recent years, a lot of researches on GPP estimation based on remote sensing data were conducted. In this study, meteorological and moderate-resolution imaging spectroradiometer (MODIS) data at A'rou (AR) freeze/thaw observation station, which is located in upper stream of Heihe River Basin, was collected to drive four remote-sensing based GPP models: Vegetation Photosynthesis Model (VPM), Temperature and Greenness model (TG), Vegetation Index model (VI) and Eddy Covariance-Light Use Efficiency model (EC-LUE). GPP observed by Eddy Covariance (EC) was used to validate the results from the four models. It is indicated that GPP, NEE and ER at AR station were 804.2 $gC/m^2/yr$, 129.6 $gC/m^2/yr$ and 673.6 $gC/m^2/yr$, respectively in 2009, indicating that 83.8% of carbon fixed by photosynthesis was released to atmosphere by ecosystem respiration. All the four models can predict GPP of alpine meadow very well. Determination coefficient between observed GPP and predicted GPP was larger than 0.94 in 2009, and was larger than 0.84 during growing season.

Key words: alpine meadow, gross primary productivity, light use efficiency model, MODIS, eddy covariance

CLC number: TP79 **Document code:** A

Citation format: Wang X F, Ma M G, Li X, Song Y, Tan J L, Huang G H and Yu W P. 2012. Comparison of remote sensing based GPP models at an alpine meadow site. Journal of Remote Sensing, 16(4): 751–763

1 INTRODUCTION

GPP is sum of photosynthesis performed by vegetation canopy at ecosystem scale, which is an important variable in carbon cycle study. With the increasing of spatial and temperal resolutions of remote sensing data, it is possible to monitor GPP over a large region. In recent years, a lot of researches on GPP estimation based on remote sensing data were conducted. Many remote sensing based GPP models were developed, such as GLO-PEM (Prince, et al., 1995), C-Fix (Veroustraete, et al., 2002), EC-LUE(Yuan, et al., 2007), MODIS-PSN (Running, et al., 2000; Heinsch, et al., 2002), VPM (Xiao, et al., 2004), TG (Sims, et al., 2008), and VI (Wu, et al., 2010). Each of these models has its advantages and disadvantages. Thus, model comparison is necessary, which can provide useful information about model choosing.

Eddy Covariance (EC) can directly measure Net Ecosystem Exchange (*NEE*) between ecosystem and atmosphere within the source area. Combining *NEE* and in-situ meteorological data, GPP can be estimated (Wohlfahrt, et al., 2005). Size of footprint is close to spatial scale of remote sensing data, so GPP observed by EC is widely used to validate remote sensing based GPP models. A lot of flux observing nets were built in the world, such as AmeriFlux, CarboEurope, ChinaFlux, to observe flux of different ecosystem and provide validation data to remote sensing based GPP models.

2 DATA AND METHOD

2.1 Study site

A'rou (AR) freeze/thaw observation station is located in the upper stream of Heihe River Basin (Fig. 1). Area around the site is flat and has homogeneous surface cover type. Geographical coordinate of the site is 100°27′52.9″E /38°02′39.8″N, and altitude of the site is 3033 m. The observation variables included the following: wind speed and direction (measured at heights of 2 m and 10 m), air temperature and humidity (measured at heights of 2 m and 10 m), air pressure, rainfall, the four components of radiation, soil temperature and moisture profiles (measured at depths of 10 cm, 20 cm, 40 cm, 80 cm, 120 cm and 160 cm), and EC (measured at a height of 3.17 m) (Li, et al., 2008). Surface cover type is alpine meadow. The height of the meadow is 20—30 cm in peak growing season. Yearly average air temperature of the site is –0.3℃, and yearly rainfall is 451 mm in 2009. Plant growing season start from May and end in September. Fig. 1 shows location of AR station, the background image is TM data acquired in July 2010.

Received: 2011-08-01; **Accepted:** 2012-01-01

Foundation: National Basic Research Program(973 program) (No.2009CB421305); Knowledge Innovation Program of the Chinese Academy of Sciences (No. KZCX2-EW-312); National High Technology Research and Development Program of China (863 program)

First author biography: WANG Xufeng (1984—), male, Ph.D. candidate. He majors in ecology modeling and carbon cycle data assimilation and has published 3 papers. E-mail: wxfgis2002@sina.com

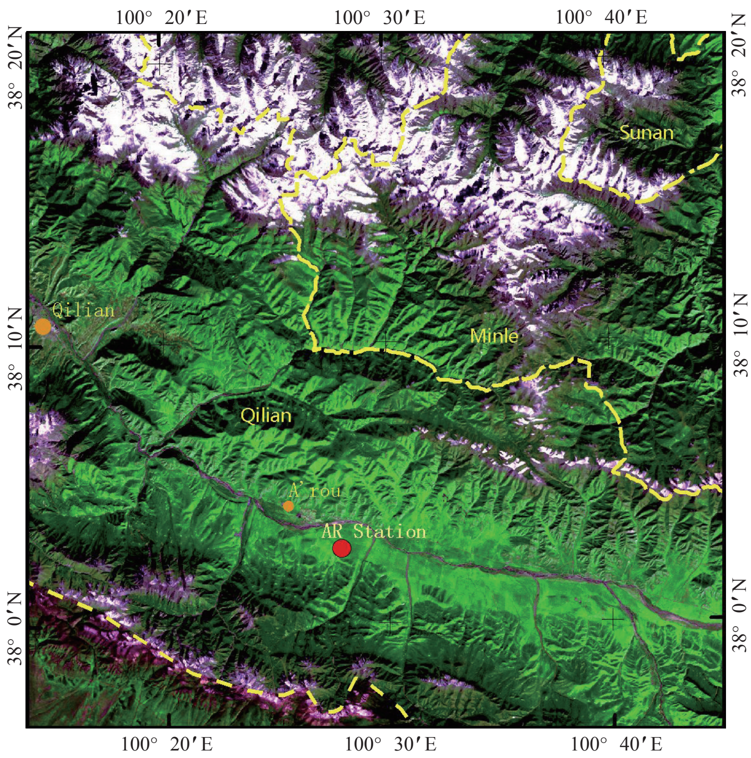

Fig. 1 Arou site in Heihe River Basin

2.2 Meteorological and Eddy Covariance data

The raw high frequency (10 Hz) data of EC was processed to produce half-hourly fluxes of CO_2, water vapour and sensible heat above canopy by using a post processing software of EdiRe (developed by Edinburgh University, UK). The processing steps included coordinate rotation, time lag correction, frequency response correction and the Webb-Pearman-Leuning (WPL) correction (Zhang, et al., 2010). Then, half-hourly flux values were excluded if sensor variance was excessive, rain was falling, incomplete sample periods, or instrument malfunction. At night, the quality of flux data is often not good because of weak turbulent mixing which has a low friction velocity (u*). Thus nighttime (downward short wave radiation <1 w/m^2) half-hourly data flux values were excluded if the friction velocity is lower than a threshold. The threshold was set to 0.1m/s for AR station (Wang, et al., 2011; Zhu, et al., 2006; Richardson&Hollinger, 2007). To obtain complete daily and annual estimates of CO_2 exchange, data gaps were filled using following method. Daytime missing *NEE* values were estimated with Michaelis–Menten equation (Eq. (1)). Nocturnal missing *NEE* values were estimated from Van't Hoff function (Eq. (2)). For the gaps, which Photosynthetically Active Radiation (PAR) and temperature data were missing, were filled with the average value of the same time in adjacent 10 days (Yan, et al., 2009).

$$NEE = \frac{\alpha \times PAR \times GEE_{max}}{\alpha \times PAR + GEE_{max}} - ER \qquad (1)$$

$$NEE_{night} = R_{ref,10} \times Q_{10}^{(T-10)/10} \qquad (2)$$

where NEE_{night} is nocturnal *NEE*. $R_{ref,10}$ is respiration rate at 10 degree Celsius, Q_{10} is the change in the rate of respiration with temperature. *T* is soil temperature, α is initial slope of the Hyperbola. GEE_{max} is maximum gross ecosystem exchange. *PAR* is photosynthetically active radiation, *ER* is ecosystem respiration.

GPP is sum of daytime *NEE* and *ER* (Eq. (3)). Nocturnal *NEE* is usually considered as *ER* at night. The function between *ER* and environmental factors (soil temperature, air temperature and so on) can be established with *NEE* and environmental factors at night, then using the function to calculate daytime *ER* with daytime observed environmental factors. Combining daytime *NEE* and *ER*, GPP can be estimated.

$$\mathrm{GPP} = NEE + ER \qquad (3)$$

2.3 MODIS data

Moderate-Resolution Imaging Spectroradiometer (MODIS) is a sensor onboard the Terra and Aqua which were launched by NASA. One satellite can overpass the study site twice in one day. It has 36 bands; the first seven bands were designed for land surface vegetation study. MOD09A1 is MODIS reflectance product of the first seven bands. The temporal resolution of MOD09A1 is 8 days and spatial resolution is 500 m. MOD11A2 is MODIS Land Surface Temperature (LST) product. Those two datasets were downloaded from NASA website, and the LST and reflectance value of the pixel which contain study site were extracted according to coordinate of the site in 2009. EVI, NDVI and Land Surface Water Index (LSWI) were calculated using extracted reflectance value of blue band (459—479 nm), red band (620—670 nm), near infrared band (841—875 nm) and shortwave infrared band (1628—1652 nm) with following equation (Eq. (4)—Eq. (6)).

$$\mathrm{EVI} = 2.5 \times (\rho_{nir} - \rho_{red}) / (\rho_{nir} + (6 \times \rho_{red} - 7.5 \times \rho_{blue}) + 1) \qquad (4)$$

$$\mathrm{NDVI} = (\rho_{nir} - \rho_{red}) / (\rho_{nir} + \rho_{red}) \qquad (5)$$

$$\mathrm{LSWI} = (\rho_{\mathrm{nir}} - \rho_{\mathrm{swir}})/(\rho_{\mathrm{nir}} + \rho_{\mathrm{swir}}) \tag{6}$$

where ρ_{blue}, ρ_{red}, ρ_{nir} and ρ_{swir} are reflectance of blue band, red band, near infrared band and shortwave infrared band respectively.

2.4 Remote Sensing based GPP model

2.4.1 VPM Model

Vegetation Photosynthesis Model (VPM) is developed by Xiao, et al. (2004, 2005), and its equations are shown as below.

$$\mathrm{GPP} = \varepsilon_0 \times f(T) \times f(W) \times f(P) \times fAPAR_{\mathrm{chl}} \times PAR \tag{7}$$

$$fAPAR_{\mathrm{chl}} = a \times \mathrm{EVI} \tag{8}$$

$$f(T) = \frac{(T - T_{\min})(T - T_{\max})}{(T - T_{\min})(T - T_{\max}) - (T - T_{\mathrm{opt}})^2} \tag{9}$$

$$f(W) = \frac{1 + \mathrm{LSWI}}{1 + \mathrm{LSWI}_{\max}} \tag{10}$$

where $fAPAR_{\mathrm{chl}}$ is the fraction of photosynthetically active radiation and is estimated with EVI; PAR is photosynthetically active radiation; ε_0 is maximum light use efficiency. In this study, ε_0 was set to 1.6 gC/MJ APAR based on an analysis of PAR and GPP during peak growing season (from the end of June to early July). $f(T)$, $f(W)$ and $f(P)$ simulate impact of temperature, water and phenology on GPP. $T_{\max}$, $T_{\min}$ and T_{opt} are maximum, minimum and optimum photosynthesis temperature. When temperature is greater than $T_{\max}$ or lower than $T_{\min}$, $f(T)$ is assigned 0. In this study, $T_{\max}$, $T_{\min}$ are set to 35℃, 0℃ respectively (Li, et al., 2006). The average air temperature 12℃ at July was used as T_{opt} (Wu, 2002). LSWI is Land Surface Water Index. $\mathrm{LSWI}_{\max}$ is maximum LSWI during growing season, and its value is 0.34 in this study (Xiao, et al., 2004, 2005). For grassland, $f(P)$ equals to 1 (Xiao, et al., 2004, 2005).

2.4.2 TG Model

Temperature and Greenness model (TG) model was developed by Sims in 2008. Its equations are given as below.

$$\mathrm{GPP} = m \times ScaledEVI \times ScaledLST \tag{11}$$

$$ScaledEVI = \mathrm{EVI} - 0.1 \tag{12}$$

$$ScaledLST = \min\left[\frac{\mathrm{LST}}{30}, (2.5 - (0.05 \times \mathrm{LST}))\right] \tag{13}$$

when EVI lower than 0.1, set $ScaledEVI$=0. If LST lower than 0℃ or greater than 50℃, set $ScaledLST$ =0. m is a scalar with unit of gC/m^2/8d. In this study m is calibrated with GPP data from the end of June to early July and its value is 140.97 gC/m^2/8d (Sims, et al., 2008).

2.4.3 VI Model

Vegetation Index model (VI) was developed by Wu, et al. in 2010. Its equations are given as below.

$$\mathrm{GPP} = a \times \mathrm{EVI} \times \mathrm{EVI} \times PAR \tag{14}$$

where a is scalar which convert PAR to GPP. In this study a is calibrated with GPP data from the end of June to early July and its value is 2.38 gC/MJ (Wu, et al., 2010).

2.4.4 EC-LUE Model

EC-LUE(Eddy Covariance-Light Use Efficiency model)is developed by Yuan, et al. in 2007. Its equations are given as below.

$$\mathrm{GPP} = \varepsilon_0 \times \min(f(T), f(W)) \times fAPAR \times PAR \tag{15}$$

$$fAPAR = 1.24 \times \mathrm{NDVI} - 0.168 \tag{16}$$

$$f(W) = \frac{LE}{HS + LE} \tag{17}$$

where ε_0 and $f(T)$ are same with that in VPM. LE is Latent Heat flux. HS is Sensible Heat flux (Yuan, et al., 2007, 2010).

3 RESULTS

3.1 Seasonal dynamics of carbon flux at AR station

Fig. 2 shows seasonal dynamics of GPP, *NEE* and *ER* at AR station in 2009. GPP was close to zero during non-growing season. It started to increase at middle April and reached peak value at end of June and early July, then started to decrease and at middle October it was close to zero again. In non-growing season, all leaves fell, so the GPP is close to zero. During growing season, GPP was increasing with the increasing of Leaf Area Index (LAI). *NEE* had two valleys during a year and was close to zero in winter. *NEE* started to decrease in early March, and reached first valley at end of April, then started to increase and reached peak value at end of June and early July. The second *NEE* valley appeared in early October, then *NEE* started to increase to about zero at middle November. *ER* has the same seasonal dynamics with GPP, but the phase of *ER* was different from that of GPP. Increase of *ER* was earlier than that of GPP and decrease of *ER* was later than that of GPP. During 2009, the maximum 8-day integrated value of GPP, *NEE* and *ER* at AR station were 64 gC/m^2/8d, 26.5 gC/m^2/8d and 41.2 gC/m^2/8d, respectively. Year sum of GPP, *NEE* and *ER* were 804.2 gC/m^2/yr, 129.6 gC/m^2/yr and 673.6 gC/m^2/yr, respectively. 83.8% of carbon fixed by photosynthesis was released to atmosphere by ecosystem respiration. Li estimated GPP of alpine meadow at Heibai station was about 789.2 gC/m^2/yr, which is close to GPP at AR station (Li, et al., 2007). Alpine meadow had higher GPP compared with other grassland ecosystem in north China. GPP of temperate grassland ecosystem in Inner Mongolia is 603 gC/m^2/yr (Wu, et al., 2008). GPP of degrade grassland at Tongyu is 304 gC/m^2/yr (Wang, et al., 2010). GPP of grassland at Sanjiangyuan Region of the Qinghai-Tibetan Plateau is about 480 gC/m^2/yr (Wu, et al., 2010).

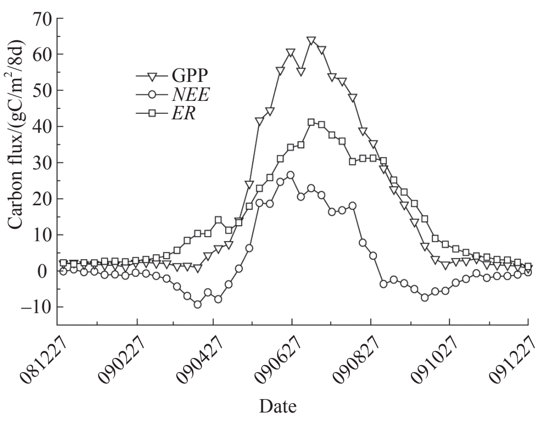

Fig. 2 Plot of GPP, NEE and RE at A'rou station in 2009

3.2 Relationship between GPP and model inputs

Fig. 3 shows seasonal dynamics of NDVI, EVI and LSWI at AR station in 2009. NDVI was the greatest, and LSWI was the lowest in the three vegetation indices. Vegetation indices had the same seasonal trends with GPP. From Table 1, we can see that determination coefficient between EVI and GPP was the highest, but that between LSWI and GPP was lowest at whole year. In winter of 2009, the abrupt change was caused by snow. Snow has high reflectance at red band and high absorption rate at shortwave band. Thus, the value of NDVI and LSWI changed abruptly. This is one of the reasons that NDVI and LSWI had lower determination coefficient with GPP compared with EVI. Better correlation between GPP and EVI than NDVI was also reported by other researchers (Huete, et al., 2002; Rahman, et al., 2005; Xiao, et al., 2004; Wu, et al., 2010).

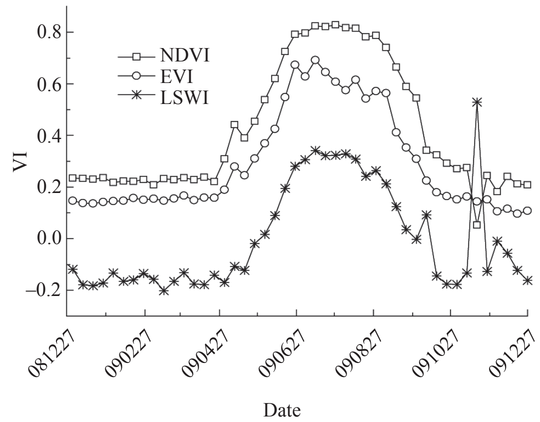

Fig. 3 Plot of NDVI, EVI and LSWI at A'rou station in 2009

Fig. 4 shows seasonal dynamics of average air temperature (Ta_2m_avg) and MODIS LST product (LST_daytime) at AR station in 2009. MODIS LST was higher than average air temperature. Average air temperature reached its peak value in July, but MODIS LST reached its peak value in May. Determination coefficient between GPP and average air temperature was far higher than that of MODIS LST (Table 1).

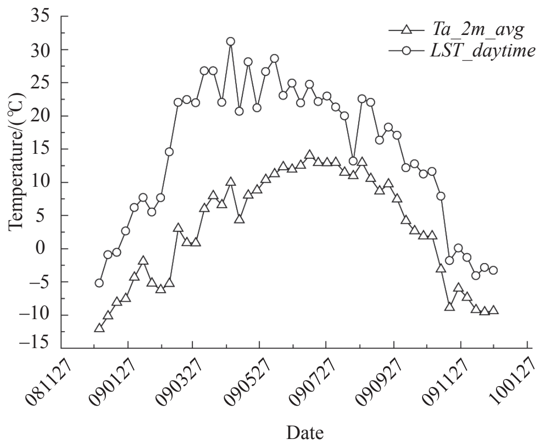

Fig. 4 Plot of mean air temperature and MODIS Land Surface Temperature at A'rou station in 2009

Table 1 R^2 between observed GPP and model inputs

	PAR	*Ta_avg*	LST	NDVI	EVI	LSWI	*HS*	*LE*
WY	0.237	0.597	0.294	0.875	0.93	0.657	0.004	0.81
GS	0.0004	0.731	0.003	0.65	0.771	0.65	0.589	0.586

WY: Whole year; GS: Growing season (May to September)

Fig. 5 shows seasonal dynamics of *PAR*, *HS* and *LE* at AR station in 2009. *PAR* and *LE* only had one peak during a year, but *HS* had two peaks. Both *PAR* and *LE* reached their peak values at the end of June and early July. Determination coefficient between *PAR* and GPP is low, and even close to 0 during growing season (Table 1). Determination coefficient between *LE* and GPP in 2009 was higher than that during growing season. Determination coefficient between *HS* and GPP in 2009 was close to 0, but that during growing season was high (Table 1).

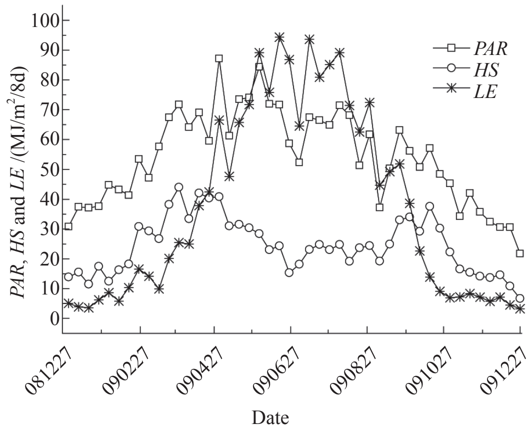

Fig. 5 Plot of *PAR*, *LE* and *HS* at A'rou station in 2009

3.3 Comparison of predicted GPP

Fig. 6 shows seasonal dynamics of GPP observed by EC and predicted by four models. All of the four models can simulate GPP dynamics correctly at alpine meadow. In 2009, GPP observed by EC was 804.2 gC/m^2/yr, VPM, EC-LUE, VI and TG predicted GPP were 778.2 gC/m^2/yr, 899.6 gC/m^2/yr, 816.4 gC/m^2/yr and 848.8 gC/m^2/yr. During growing season in 2009, GPP observed by EC is 747gC/m^2/yr, VPM, EC-LUE, VI and TG predicted GPP were 732.4 gC/m^2/yr, 859.5 gC/m^2/yr, 749.3 gC/m^2/yr and 780.8 gC/m^2/yr. GPP predicted by VPM and VI model were very close to the observed value of EC. The order of R square of the four models is: VPM>VI>EC-LUE>TG (Fig. 7 and Table 2). Determination coefficient values of the four models were greater than 0.94 in 2009, and were greater than 0.84 during growing season. That means all of the four models had good performance at AR station.

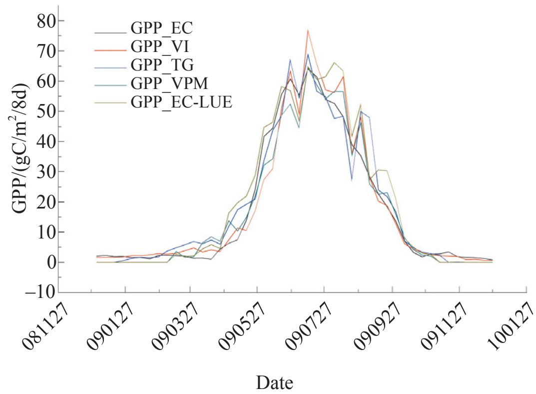

Fig. 6 Plot of GPP observed by EC and GPP predicted by models at A'rou station in 2009

Table 2 Comparison between EC observed GPP and model predicted GPP

		GPP_VPM	GPP_EC-LUE	GPP_TG	GPP_VI	GPP_EC
WY	R^2	0.9571	0.9483	0.9408	0.9508	/
	a	0.9474	1.0643	0.9751	1.0154	/
	b	0.3536	0.9489	1.4057	–0.0048	/
	GPP	778.2	899.6	848.8	816.4	804.2
GS	R^2	0.8944	0.8816	0.844	0.8822	/
	a	0.8586	0.8362	0.8546	1.0638	/
	b	4.5496	11.745	7.1181	–2.2719	/
	GPP	732.4	859.5	780.8	749.3	747

WY: Whole year; GS: Growing season (May to September)

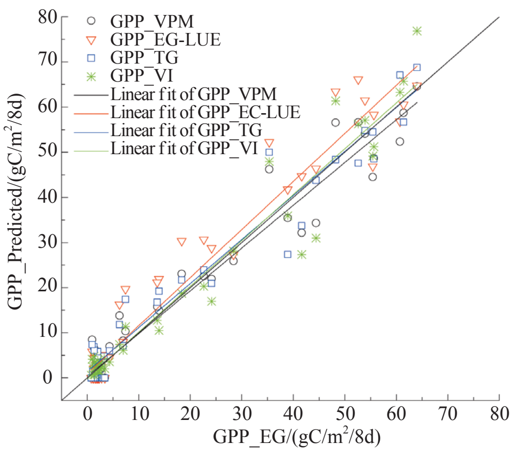

Fig. 7 Scatter plot of GPP observed by EC and GPP predicted by models at A'rou station in whole 2009

4 DISCUSSIONS AND CONCLUSIONS

In this study, GPP of an alpine meadow site was estimated with EC and remote sensing based models, and accuracy of these models was assessed.

EC can directly measure *NEE* between ecosystem and atmosphere, and is widely used to monitor temporal dynamic of carbon flux and provides validation data to carbon flux modeling. Using EC data to validate remote sensing based GPP model, uncertainties from three aspects must be considered. (1) Due to environment interrupt and equipment malfunction, there are errors in EC data, so rigid post processing must be performance before using. To obtain daily or yearly integrated GPP, Gaps in the data must be filled, this will result errors to EC observed data. (2) The mismatch of spatial scale will result in uncertainties. EC observe GPP over a footprint whose size and shape changes with the observation height of EC, wind speed and wind direction. However, GPP model simulate GPP over a pixel which has regular shape. (3) GPP is estimated using EC observed *NEE* and temperature data. The estimation method neglect light respiration during daytime. The also result in uncertainties.

Among the models' inputs, vegetation indices had the highest determination coefficient with observed GPP, followed by air temperature, LE, HS, PAR and LST. Vegetation indices reflect the status of vegetation, so they have high determination coefficients. Air temperature affects photosynthesis and LE can reflect water condition of vegetation, so they also are highly correlated with GPP. HS has two peaks during a year, but GPP only has one, so the determination coefficient is low in whole year; however, during growing season, HS and GPP has the opposite trend and has relative high determination coefficient. PAR and GPP has low determination coefficient, which means light used for plant photosynthesis is adequate. Low determination coefficient between MODIS LST and GPP maybe resulted from two aspects: (1) MODIS LST is a mix pixel which contains soil and vegetation, and ratio of each component changes with growing of vegetation; (2) clouds and aerosol impact on LST retrieval.

Inputs of VPM, EC-LUE and VI not only include meteorological data, but also include remote sensing data. EVI is use to estimate GPP in VPM and VI, but NDVI is used in EC-LUE. EVI is reported has better correlation with GPP than NDVI, this is a reason that EC-LUE has lower R^2 than VPM and VI at AR site. In this study, HS and LE data used in EC-LUE model were from EC observations, and there is an energy balance closure problem in EC system, so using HS and LE observed by EC as inputs of EC-LUE also result in uncertainties in GPP estimation. TG is an entirely Remote Sensing based GPP model, it does not need any meteorological inputs. Its inputs include EVI and LST. LST retrial usually is affected by clouds and aerosol, so it will result in uncertainties in GPP estimation using TG model. VI and TG model have relative simple form and need less input data. When predicting GPP over a large region, TG and VI are suitable to be used and avoid the uncertainties from grid meteorological data. Zhao, et al. (2006) used different meteorological force data (NASA DAO, NCEP and ECMWF) to drive MODIS-PSN and found that the result is obvious different, that means there are great uncertainties in meteorological force data in large scale. To simulate GPP at site scale using meteorological observations, VPM and EC-LUE are suitable, because they have relative higher accuracy.

From this study, the following conclusion can be drawn: (1) GPP, *NEE* and *ER* of AR station were: 804.2 gC/m²/yr, 129.6 gC/m²/yr and 673.6 gC/m²/yr respectively in 2009. 83.8% of carbon fixed through photosynthesis was released to atmosphere by ecosystem respiration; (2) All the four Remote Sensing base GPP models can correctly simulate GPP at alpine meadow, and the maximum determination coefficient value is 0.9571 (VPM model) and minimum determination coefficient value is 0.9408 (TG model) during the whole year. During growing season, determination coefficient values of the four models were higher than 0.84.

REFERENCES

Heinsch F A, Reeves M, Votava P, Kang S, Milesi C, Zhao M S, Glassy J, Jolly W M, Loehman R, Bowker C F, Kimball J S, Nemani R R and Running S W. 2002. User's Guide GPP and NPP (MOD17A2/A3) Products NASA MODIS Land Algorithm. [2010-12-17] http://modis.gsfc.nasa.gov/

Huete A, Didan K, Miura T, Rodriguez E P, Gao X and Ferreira L G. 2002. Overview of the radiometric and biophysical performance of the MODIS vegetation indices. Remote Sensing of Environment, 83(1/2): 195–213 [DOI: 10.1016/S0034-4257(02)00096-2]

Li X, Ma M G, Wang J, Liu Q, Che T, Hu Z Y, Xiao Q, Liu Q H, Su P X, Chu R Z, Jin R, Wang W Z and Ran Y H. 2008. Simultaneous remote sensing and ground-based experiment in the Heihe river basin: scientific objectives and experiment design. Advances in Earth Science, 23(9): 897–913

Li Z Q, Yu G R, Xiao X M, Li Y N, Zhao X Q, Ren C Y, Zhang L M and Fu Y L. 2007. Modeling gross primary production of alpine ecosystems in the Tibetan Plateau using MODIS images and climate data. Remote Sensing of Environment, 107(3): 510–519 [DOI: 10.1016/j.rse.2006.10.003]

Prince S D and Goward S N. 1995. Global primary production: a remote sensing approach. Journal of Biogeography, 22(4/5): 815–835 [DOI: 10.2307/2845983]

Rahman A F, Sims D A, Cordova V D and El-Masri B Z. 2005. Potential of MODIS EVI and surface temperature for directly estimating per-pixel ecosystem C fluxes. Geophysical Research Letters, 32, L19404: 1–4 [DOI: 10.1029/2005GL024127]

Richardson A D and Hollinger D Y. 2007. A method to estimate the additional uncertainty in gap-filled NEE resulting from long gaps in the CO_2 flux record. Agricultural and Forest Meteorology, 147(3/4): 199–208 [DOI: 10.1016/j.agrformet.2007.06.004]

Running S W, Thornton P E, Nemani R and Glassy J M. 2000. Global terrestrial gross and net primary productivity from the earth observing system // Sala O E, Jackson R B, Mooney H A and Howarth R W, eds. Methods in Ecosystem Science. New York: Springer-Verlag: 44–57

Sims D A, Rahman A F, Cordova V D, El-Masri B Z, Baldocchi D D, Bolstad P V, Flanagan L B, Goldstein A H, Hollinger D Y, Misson L, Monson R K, Oechel W C, Schmid H P, Wofsy S C and Xu L K. 2008. A new model of gross primary productivity for North American ecosystems based solely on the enhanced vegetation index and land surface temperature from MODIS. Remote Sensing of Environment, 112(4): 1633–1646 [DOI: 10.1016/j.rse.2007.08.004]

Veroustraete F, Sabbe H and Eerens H. 2002. Estimation of carbon mass fluxes over Europe using the C-Fix model and Euroflux data. Remote Sensing of Environment, 83(3): 376–399 [DOI: 10.1016/S0034–4257(02)00043–3]

Wang X F, Ma M G, Huang G H, Veroustraete F, Zhang Z H, Song Y and Tan J L. 2011. Vegetation primary production estimation at maize and alpine meadow over the Heihe River Basin, China. International Journal of Applied Earth Observation and Geoinformation, (In press) [DOI: 10.1016/j.jag.2011.09.009]

Wang Z, Xiao X M and Yan X D. 2010. Modeling gross primary production of maize cropland and degraded grassland in northeastern China. Agricultural and Forest Meteorology, 150(9): 1160–1167 [DOI: 10.1016/j.agrformet.2010.04.015]

Wohlfahrt G, Bahn M, Haslwanter A, Newesely C and Cernusca A. 2005. Estimation of daytime ecosystem respiration to determine gross primary production of a mountain meadow. Agricultural and Forest Meteorology, 130(1/2): 13–25 [DOI: 10.1016/j.agrformet.2005.02.001]

Wu C Y, Han X Z, Ni J S, Niu Z and Huang W J. 2010. Estimation of gross primary production in wheat from in situ measurements. International Journal of Applied Earth Observation and Geoinformation, 12(3): 183–189 [DOI: 10.1016/j.jag.2010.02.006]

Wu L B, Gu S, Zhao L, Xu S X, Zhou H K, Feng C, Xu W X, Li Y N, Zhao X Q and Tang Y H. 2010. Variation in net CO_2 exchange, gross primary production and its affecting factors in the planted pasture ecosystem in Sanjiangyuan Region of the Qinghai-Tibetan Plateau of China. Chinese Journal of Plant Ecology, 34(7): 770–780

Wu W H. 2002. Plant Physiology. Beijing: Science Press: 172–173

Wu W X, Wang S Q, Xiao X M, Yu G R, Fu Y L and Hao Y B. 2008. Modeling gross primary production of a temperate grassland ecosystem in Inner Mongolia, China, using MODIS imagery and climate data. Science in China Series D: Earth Sciences, 51(10): 1501–1512

Xiao X M, Hollinger D, Aber J, Goltz M, Davidson E A, Zhang Q Y and Moore B III. 2004. Satellite-based modeling of gross primary production in an evergreen needleleaf forest. Remote Sensing of Environment, 89(4): 519–534 [DOI: 10.1016/j.rse.2003.11.008]

Xiao X M, Zhang Q Y, Hollinger D, Aber J and Moore B. 2005. Modeling gross primary production of an evergreen needleleaf forest using MODIS and climate data. Ecological Applications, 15(3): 954–969 [DOI: 10.1890/04-0470]

Yan H M, Fu Y L, Xiao X M, Huang H Q, He H L and Ediger L. 2009. Modeling gross primary productivity for winter wheat-maize double cropping system using MODIS time series and CO_2 eddy flux tower data. Agriculture, Ecosystems and Environment, 129(4): 391–400 [DOI: 10.1016/j.agee.2008.10.017]

Yuan W P, Liu S G, Zhou G H, Zhou G Y, Tieszen L L, Baldocchi D, Bernhofer C, Gholz H, Goldstein A H, Goulden M L, Hollinger D Y, Hu Y M, Law B E, Stoy P C, Vesala T and Wofsy S C. 2007. Deriving a light use efficiency model from eddy covariance flux data for predicting daily gross primary production across biomes. Agricultural and Forest Meteorology, 143(3/4): 189–207 [DOI: 10.1016/j.agrformet.2006.12.001]

Yuan W P, Liu S G, Yu G R, Bonnefond J M, Chen J Q, Davis K, Desai A R, Goldstein A H, Gianelle D, Rossi F, Suyker A E and Verma S B. 2010. Global estimates of evapotranspiration and gross primary production based on MODIS and global meteorology data. Remote Sensing of Environment, 114(7): 1416–1431 [DOI: 10.1016/j.rse.2010.01.022]

Zhang Z H, Wang W Z, Ma M G, Xu Z W, Wu Y R, Huang G H and Tan J L. 2010. Data processing and product analysis of eddy covariance flux data for WATER. Remote Sensing Technology and Application, 25(6): 788–796

Zhao M S, Running S W and Nemani R R. 2006. Sensitivity of Moderate Resolution Imaging Spectroradiometer (MODIS) terrestrial primary production to the accuracy of meteorological reanalyses. Journal of Geophysical Research, 111: G01002 [DOI: 10.1029/2004JG000004]

Zhu Z L, Sun X M, Wen X F, Zhou Y L, Tian J and Yuan G F. 2006. Study on the processing method of nighttime CO_2 eddy covariance flux data in ChinaFLUX. Science in China Series D: Earth Sciences. 49(Supp. II): 36–46 [DOI: 10.1007/s11430-006-8036-5]

遥感GPP模型在高寒草甸的应用比较

王旭峰[1,2]，马明国[1]，李新[1]，宋怡[1,2]，谭俊磊[1]，黄广辉[1]，于文凭[1,2]

1. 中国科学院 寒区旱区环境与工程研究所 寒旱区遥感观测系统试验站，甘肃 兰州 730000；
2. 中国科学院 研究生院，北京100049

摘　要：随着遥感数据时空分辨率的提高，大范围实时监测总初级生产力GPP(Gross Primary Productivity)的变化成为可能。本研究收集了黑河流域阿柔冻融观测站的气象观测资料和MODIS数据，驱动VPM、TG、VI和EC-LUE 4个模型估算了该站点的GPP，并应用涡动相关观测的GPP验证了模拟结果，并比较了这4个模型的模拟精度。结果表明：阿柔站2009年的涡动相关观测的GPP、NEE(Net Ecosystem Exchange)和ER(Ecosystem Respiration)分别为：804.2 gC/m^2/yr、129.6 gC/m^2/yr和 673.6 gC/m^2/yr。该站点光合作用固定的碳有83.8%通过生态系统的呼吸作用释放到大气中。基于遥感的GPP模型能够很好地模拟高寒草甸的GPP，全年的判定系数在0.94以上，生长季的判定系数大于0.84。

关键词：高寒草甸，总初级生产力，光能利用率模型，MODIS，涡动相关观测系统

中图分类号：TP79　　**文献标志码**：A

引用格式：王旭峰，马明国，李新，宋怡，谭俊磊，黄广辉，于文凭．2012．遥感GPP模型在高寒草甸的应用比较．遥感学报，16(4): 751–763

Wang X F, Ma M G, Li X, Song Y, Tan J L, Huang G H and Yu W P. 2012. Comparison of remote sensing based GPP models at an alpine meadow site. Journal of Remote Sensing, 16(4): 751–763

1 引　言

总初级生产力GPP可以反映植被通过光合作用吸收碳的能力。它是碳循环研究中一个非常关键的变量。随着遥感数据时空分辨率的提高，大范围实时监测GPP的变化成为可能。近年来国内外开展了大量的基于遥感的GPP估算研究，也发展了很多基于遥感的GPP估算模型，如GLO-PEM (Prince和Goward，1995)、C-Fix (Veroustraete 等，2002)、EC-LUE(Yuan 等，2007)、MODIS-PSN(Running 等，2000；Heinsch 等，2002)、VPM(Xiao 等，2004)、TG(Sims 等，2008)、VI(Wu 等，2010)等。这些模型都是依据光能利用率理论，结合遥感观测的植被指数以及实测的气象观测资料来估算生态系统的GPP。基于不同的考虑，每个模型选取的环境限制因子特点不同，对这些模型进行比较研究可为模型的选择应用提供参考信息。

涡动相关技术可以直接观测净生态系统交换量*NEE*(Net Ecosystem Exchange)。通过NEE和辅助气象数据可以计算出观测站点的GPP(Wohlfahrt 等，2005)。而且通过涡动相关获得的是一个贡献源区(Footprint)内的GPP，在空间尺度上和遥感估算比较接近。它被广泛地用来验证基于遥感的GPP估算模型。现已建立很多的通量观测网络(如AmeriFlux, CarboEurope和ChinaFlux等)，针对各种生态系统的碳通量进行观测，为遥感GPP模型的发展提供了大量可靠数据。

2 数　据

2.1 研究站点

阿柔冻融观测站(阿柔站)位于黑河上游支流八宝河南侧的河谷高地上，试验场周围地势相对

收稿日期：2011-08-01；**修订日期**：2012-01-01

基金项目：国家重点基础研究发展计划(973计划)(编号: 2009CB421305)；中国科学院知识创新工程重要方向项目(编号: KZCX2-EW-312)；国家高技术研究发展计划(863计划)(编号: 2009AA122104)

第一作者简介：王旭峰(1984—　)，男，博士研究生，现从事生态遥感、碳通量模拟及碳数据同化方面的研究，已发表论文3篇。E-mail: wxfgis2002@sina.com。

平坦开阔，下垫面比较均一。站点的地理坐标为(100° 27′ 52.9″ E，38° 02′ 39.8″ N)，海拔高度为3033 m。主要观测变量有风温湿梯度观测(2 m和10 m)、气压、降水；四分量辐射；土壤剖面：温度、水分(10 cm、20 cm、40 cm、80 cm、120 cm和160 cm)及土壤热通量(5 cm和15 cm)；涡动相关(3.17 m)(李新 等，2008)。下垫面为高寒草甸，植被高度为20—30 cm。2009年平均气温为－0.3℃，年降雨量为451 mm。5月—9月为植被的生长季。图1显示的阿柔站点的位置分布，背景影像为2010年7月份的TM影像。

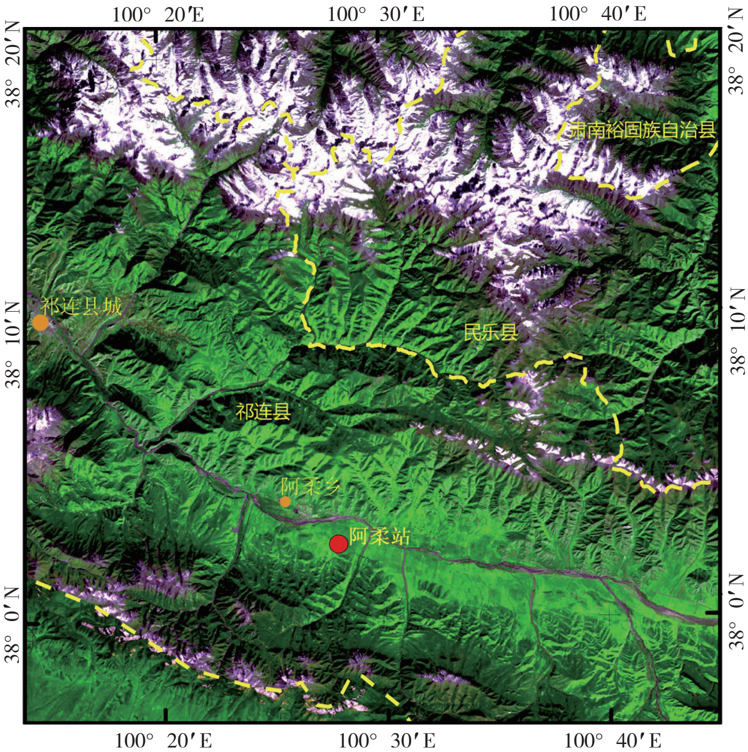

图1 阿柔站点位置图

2.2 气象和涡动数据

应用Edire软件对阿柔站2009年全年的涡动数据进行了异常值剔除(降雨时刻，野点t仪器故障)，坐标旋转，WPL校正，频率响应订正(张智慧 等，2010)，夜间资料(下行辐射<1 w/m^2)进行U*校正，临界值取0.1 m/s(Zhu 等，2006；Richardson和Hollinger，2007；Wang 等，2011)。并对处理后的资料进行了数据插补：如果涡动资料缺失，但该时段有气象资料，在白天，根据Michaelis-Menten方程(式(1))进行填补；在夜间，根据Van’t Hoff方程(式(2))进行填补。如果涡动资料缺失，且该时段没有气象资料，则用相邻的10天中相同时刻的平均值代替(Yan 等，2009)。

$$NEE = \frac{\alpha \times PAR \times GEE_{\max}}{\alpha \times PAR + GEE_{\max}} - ER \tag{1}$$

$$NEE_{\text{night}} = R_{\text{ref},10} \times Q_{10}^{(T-10)/10} \tag{2}$$

式中，NEE_{night}是夜间生态系统的呼吸量，$R_{\text{ref},10}$是10摄氏度时生态系统的呼吸量，Q_{10}是呼吸速率随温度的变化速率，T是近地表的空气温度。α是最大光能利用效率，PAR(Photosynthetically Active Radiation)是光合有效辐射，$GEE_{\max}$是最大的总生态系统交换量，ER(Ecosystem Respiration)是生态系统呼吸量。

根据NEE和ER可以计算出GPP。一般假设夜间涡动相关观测的NEE等于ER，利用夜间的NEE建立ER与环境因子(土壤温度和空气温度等)之间的关系，然后就可以计算出白天的ER，GPP是NEE与ER之和(式(3))。

$$\text{GPP} = NEE + ER \tag{3}$$

2.3 遥感数据

中分辨率成像光谱仪MODIS是搭载在NASA发射的Terra和Aqua两颗卫星上的传感器。单星一天过境两次，白天和晚上各一次。MODIS共包含36个

波段，前7个波段主要为地表植被研究设计。MOD09A1是 MODIS前7个波段反射率的8天合成的数据产品，其空间分辨率为500 m。 MOD11A2是8天的地表温度产品，包括白天和晚上过境时刻的地表温度。我们从NASA的网站上下载了该产品，并提取了阿柔站所在像元2009年的反射率和地表温度LST，应用蓝波段(459—479 nm)，红波段(620—670 nm)，近红外波段(841—875 nm)和短波红外波段(1628—1652 nm)4个波段的反射率进行植被指数的计算。本研究中用到的植被指数包括增强植被指数EVI、归一化植被指数NDVI和陆地水分指数LSWI。计算方法如式(4)—(6)。

$$\mathrm{EVI} = 2.5\times(\rho_{\mathrm{nir}}-\rho_{\mathrm{red}})/(\rho_{\mathrm{nir}}+(6\times\rho_{\mathrm{red}}-7.5\times\rho_{\mathrm{blue}})+1) \tag{4}$$

$$\mathrm{NDVI} = (\rho_{\mathrm{nir}}-\rho_{\mathrm{red}})/(\rho_{\mathrm{nir}}+\rho_{\mathrm{red}}) \tag{5}$$

$$\mathrm{LSWI} = (\rho_{\mathrm{nir}}-\rho_{\mathrm{swir}})/(\rho_{\mathrm{nir}}+\rho_{\mathrm{swir}}) \tag{6}$$

式中，ρ_{blue}、ρ_{red}、ρ_{nir}和ρ_{swir}分别是蓝波段、红波段、近红外波段和短波红外波段的反射率。

2.4 基于遥感的GPP估算模型

2.4.1 VPM模型

VPM(Vegetation Photosynthesis Model)模型是Xiao等人(2004，2005)发展的基于遥感的GPP估算模型。表达式如下：

$$\mathrm{GPP} = \varepsilon_0\times f(T)\times f(W)\times f(P)\times fAPAR_{\mathrm{chl}}\times PAR \tag{7}$$

$$fAPAR_{\mathrm{chl}} = a\times \mathrm{EVI} \tag{8}$$

$$f(T) = \frac{(T-T_{\min})(T-T_{\max})}{(T-T_{\min})(T-T_{\max})-(T-T_{\mathrm{opt}})^2} \tag{9}$$

$$f(W) = \frac{1+\mathrm{LSWI}}{1+\mathrm{LSWI}_{\max}} \tag{10}$$

式中，$fAPAR_{\mathrm{chl}}$是冠层中叶绿素吸收的光合有效辐射吸收比，通过EVI估算。PAR是光合有效辐射，ε_0是最大光能利用率，本研究中根据对生长高峰期的PAR和GPP的分析，将其设为1.6 gC/MJ $APAR$。$f(T)$、$f(W)$ 和 $f(P)$分别是温度、水分和物候状态对光能利用效率的影响函数。$T_{\max}$、$T_{\min}$和T_{opt}分别是进行光合作用的最高、最小和最适空气温度。当T小于$T_{\min}$的时候，$f(T)$=0。本研究中高寒草甸的最高和最小温度根据文献中的值设定为35℃，0℃(Li 等，2007)，将7月份的平均空气温度设为最适光合温度T_{opt}，值为12℃(伍维华，2002)。LSWI是陆地水分指数，$\mathrm{LSWI}_{\max}$是植被生长季LSWI的最大值，在本研究中设为0.34(Xiao 等，2004，2005)。对于草地，在VPM模型中$f(P)$设为1(Xiao 等，2004，2005；Wu 等，2008)。

2.4.2 TG模型

TG(Temperature and Greenness model)模型是Sims等人(2008)发展的基于遥感的GPP估算模型，表达式如下：

$$\mathrm{GPP} = m\times ScaledEVI\times ScaledLST \tag{11}$$

$$ScaledEVI = \mathrm{EVI}-0.1 \tag{12}$$

$$ScaledLST = \min\left[\frac{\mathrm{LST}}{30},(2.5-(0.05\times\mathrm{LST}))\right] \tag{13}$$

式中，EVI为增强植被指数，当EVI小于0.1时，$ScaledEVI$=0；LST为地表温度，LST小于0℃或大于50℃时，$ScaledLST$=0；m是转换系数，随着植被类型和环境的变化而有所不同，本研究中利用6月底和7月初的GPP数据、EVI数据和LST数据，将m值标定为140.97 gC/m^2/8d。

2.4.3 VI模型

VI(Vegetation Index model)模型是Wu等人(2010)发展的基于遥感的GPP估算模型，该模型利用增强植被指数和光合有效辐射计算GPP，表达式如下：

$$\mathrm{GPP} = a\times \mathrm{EVI}\times \mathrm{EVI}\times PAR \tag{14}$$

式中，EVI是增强植被指数，PAR是光合有效辐射，a是转换系数，随着植被类型和环境的变化而有所不同，本研究中利用6月底、7月初的GPP、EVI和PAR数据，将a值标定为2.38 gC/MJ。

2.4.4 EC-LUE

EC-LUE(Eddy Covariance-Light Use Efficiency model)是Yuan等人(2007)提出的一个基于遥感的GPP模型(Yuan 等，2007，2010)，其表达式如下：

$$\mathrm{GPP} = \varepsilon_0\times\min(f(T),f(W))\times fAPAR\times PAR \tag{15}$$

$$fAPAR = 1.24\times\mathrm{NDVI}-0.168 \tag{16}$$

$$f(W) = \frac{LE}{HS+LE} \tag{17}$$

式中，ε_0，$f(T)$和VPM模型中的一样，LE是潜热，HS是显热。

3 结 果

3.1 阿柔站碳通量的季节动态

图2为经过插补后阿柔站2009年全年的GPP、NEE和ER。从图中可以看出，非生长季GPP非常小，接近0值；在4月中旬开始增加，到6月底7月初达到峰值，到10月中旬又减小至0值附近。在非生长季，牧草全部凋落，光合作用微弱，所以GPP很小，到

了生长季(5月—9月)随着植被的增长，叶面积的增加，GPP就会升高。*ER*和GPP的变化趋势一致，但是其开始增长的时间要早于GPP开始增长的时间，回到0值附近的时间要晚于GPP回到0值附近的时间。*NEE*一年内有两个谷值，冬天*NEE*在0值附近，3月初开始减小，到4月底达到最小值后开始增加，然后在6月底7月初达到峰值，之后又开始减小，到10月初达到第2个谷值，然后开始增加，在11月中旬回到0值附近。阿柔站2009年GPP、*NEE*和*ER*最大值分别为64 gC/m^2/8d、26.5 gC/m^2/8d和41.2 gC/m^2/8d；GPP、*NEE*和*ER*的年累积量分别为804.2 gC/m^2/yr、129.6 gC/m^2/yr和673.6 gC/m^2/yr。*ER*占了GPP的83.8%。Li等人(2007)在海北站用涡动获得的高寒草甸的GPP约为789.2 gC/m^2/yr，与本研究中的结果较为接近。与其他的草地生态系统相比，高寒草甸具有较高的生产力。内蒙古温带草原的GPP是603 gC/m^2/yr (Wu 等，2008)，通榆荒漠草地的GPP约为304 gC/m^2/yr (Wang 等，2010)，三江源人工草地的GPP为480 gC/m^2/yr (吴力博 等，2010)。

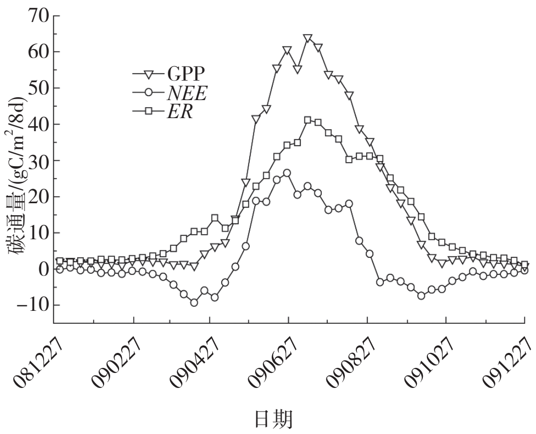

图2 涡动相关观测的阿柔站2009年GPP，*NEE*和*ER*的季节变化

3.2 GPP与模型输入因子的关系

图3是2009年阿柔站NDVI、EVI和LSWI的季节动态。在数值上NDVI最大，其次是EVI，LSWI的值最小。这3个植被指数都是在6月底7月初达到峰值，全年变化趋势与GPP的趋势一致。植被指数与GPP的判定系数为：EVI>NDVI>LSWI(表1)。NDVI和LSWI在2009年冬天的突变是由于地表被雪覆盖造成的，雪在可见光波段有较强的反射，而在短波红外波段有较强的吸收，所以NDVI在该时段突然变小而LSWI突然增大。这是导致他们与GPP的判定系数均低于EVI的原因之一。在生长季(5月—9月)NDVI和LSWI与GPP的判定系数非常接近，但是两者均明显低于EVI。许多研究者都发现EVI与GPP的相关性要好于NDVI(Huete 等，2002；Xiao 等，2004；Rahman 等，2005；Wu 等，2010)。

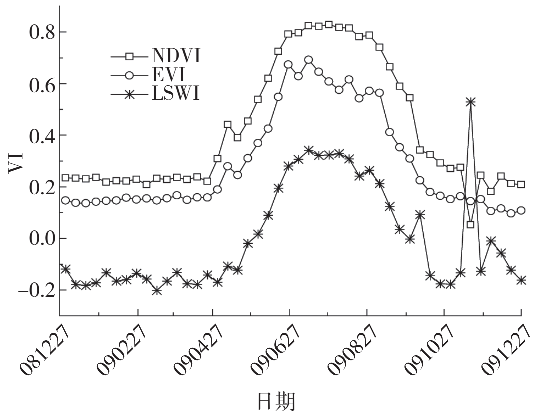

图3 阿柔站2009年的植被指数(NDVI，EVI和LSWI)

图4显示了阿柔站2009年的平均空气温度Ta_2m_avg和MODIS白天过境时刻的地表温度*LST_daytime*。MOIDS的地表温度明显高于平均空气温度。平均空气温度与GPP之间的判定系数要高于MODIS地表温度与GPP的判定系数，特别是在生长季(表1)。从图4和图2可以看出平均空气温度的变化趋势与GPP的变化趋势的一致性要好于MODIS地表温度。

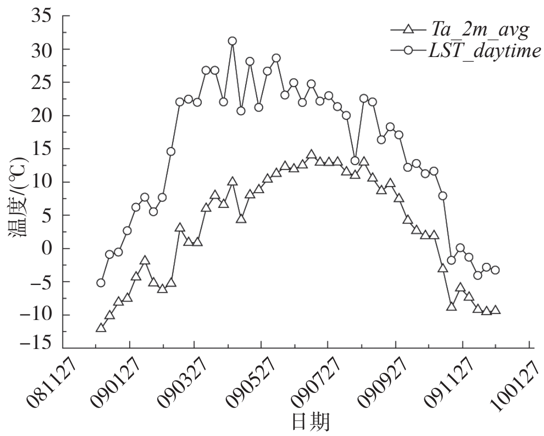

图4 *Ta_2m_avg*和*LST_daytime*

图5为*PAR*、*HS*和*LE*的季节动态。阿柔站的*PAR*是单峰曲线，生长季*PAR*要高于非生长季，峰值出现在6月底、7月初。*PAR*与GPP的判定系数很小，特别是在生长季(5月—9月)几乎为零(表1)，可能是在该研究站点光照充足，光照不是限制植被生长的最主要因子。潜热通量也是单峰曲线峰值出现在6月底、7月初，而显热是双峰曲线，峰值分别出现在4月和10月。潜热通量与GPP有很好的相关性。显热通量只在生长季与GPP有较好的相关性(表1)。

表1 GPP与环境因子的判定系数R^2

	PAR	*Ta_avg*	LST	NDVI	EVI	LSWI	*HS*	*LE*
全年	0.237	0.597	0.294	0.875	0.93	0.657	0.004	0.81
生长季	0.0004	0.731	0.003	0.65	0.771	0.65	0.589	0.586

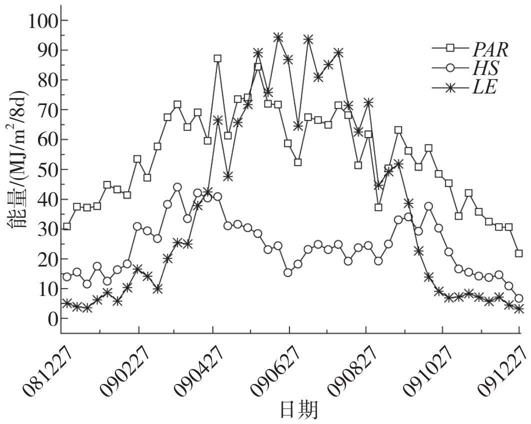

图5 阿柔站2009年的*PAR*、*HS*和*LE*

3.3 模拟GPP与涡动相关估算GPP的对比

图6为模拟的GPP与涡动相关观测估算的GPP的对比。从该图可以看出这4个模型都可以很好地模拟阿柔站的GPP的季节动态。2009年涡动相关观测的GPP为804.2 gC/m^2/yr，VPM、EC-LUE、VI和TG的模拟结果分别为778.2 gC/m^2/yr、899.6 gC/m^2/yr、816.4 gC/m^2/yr和848.8 gC/m^2/yr。2009年生长季涡动相关观测的GPP为747 gC/m^2/yr，VPM、EC-LUE、VI和TG的模拟结果分别为732.4 gC/m^2/yr、859.5 gC/m^2/yr、749.3 gC/m^2/yr和780.8 gC/m^2/yr。VPM和VI模型的模拟的GPP的年总量和生长季的总量非常接近涡动相关观测值。模拟结果与涡动相关观测的GPP的判定系数为：VPM>VI>EC-LUE>TG(图7和表2)。所有模型全年的判定系数高于生长季的判定系数，并且都在0.94以上，说明这4个模型都很好地解释了GPP的季节变化。

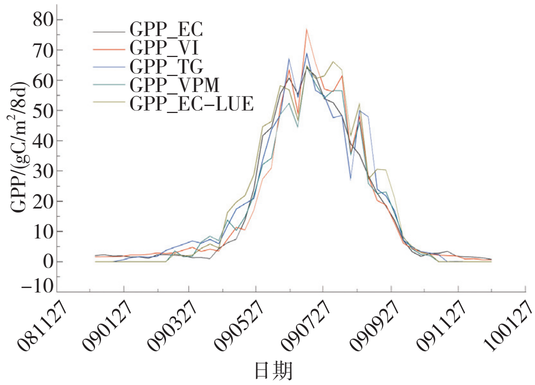

图6 阿柔站2009年的涡动相关观测的GPP和模型模拟的GPP

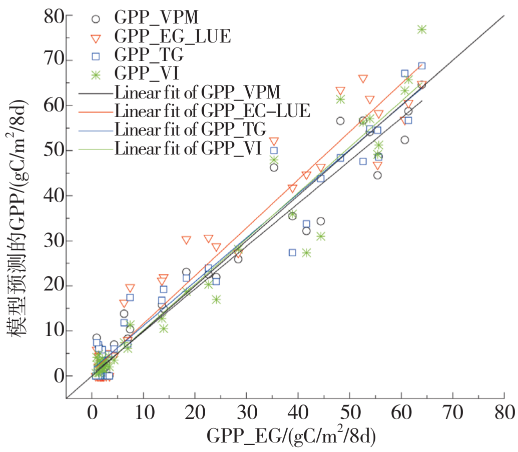

图7 涡动相关观测的GPP与模型模拟的GPP的散点图

表2 涡动相关观测GPP与模型预测GPP的比较(R^2是判定系数、*a*和*b*是线性回归的斜率和截距)

		GPP_VPM	GPP_EC-LUE	GPP_TG	GPP_VI	GPP_EC
全年	R^2	0.9571	0.9483	0.9408	0.9508	/
	a	0.9474	1.0643	0.9751	1.0154	/
	b	0.3536	0.9489	1.4057	– 0.0048	/
	GPP	778.2	899.6	848.8	816.4	804.2
生长季	R^2	0.8944	0.8816	0.844	0.8822	/
	a	0.8586	0.8362	0.8546	1.0638	/
	b	4.5496	11.745	7.1181	– 2.2719	/
	GPP	732.4	859.5	780.8	749.3	747

4 讨论与结论

本研究应用涡动相关法和光能利用率模型两种方法获得了高寒草甸的GPP。应用涡动相关获得的GPP评价4种不同的光能利用率模型的模拟精度。

涡动相关观测系统可以直接测量生态系统和大气之间的交换量，被广泛的用来定点监测生态系统碳通量的变化，并为模型验证提供数据。应用涡动相关观测的碳通量验证基于遥感数据计算的碳通量时主要有以下几方面的不确定性：

(1)由于环境干扰或者仪器故障，涡动的原始资料要经过严格的后续处理才能使用，而且需要对缺失资料进行插补，这些数据处理过程中往往会给涡动相关观测结果带来一些不确定性。

(2)空间尺度的不匹配会给计算结果的验证带来一定的不确定性。涡动相关观测的碳通量代表的是地表一定贡献源区的碳通量，而这个贡献源区的大小和形状是随着观测仪器的高度、风速和风向等不断变化的，而遥感生产力模型都是基于规则的像元进行计算的。

(3)涡动观测到的是*NEE*，而GPP和*ER*都是在温度、辐射等气象因子的辅助下估算出来的。首先根据夜间气温和夜间的*NEE*建立生态系统呼吸量和温度之间的函数关系，然后把这一函数应用到白天来计算白天的呼吸量，这就存在一定的误差。因为白天植被和微生物的生理活动更活跃，且白天有光呼吸存在，而晚上没有。

在模型输入数据中，3个植被指数与GPP的判定系数最大，其次是平均气温和潜热，再次是显热，*PAR*和LST与涡动相关观测估算的GPP的相关性最小。植被指数可以反映植被的生长状态，所以其与GPP具有很高的判定系数。气温直接影响植被的光合作用，潜热可以反映植被的水分状态，所以它们与GPP也具有较高的判定系数。从全年来看显热与GPP的变化趋势不太一致，而在生长季显热与GPP的变化趋势刚好相反，所以在生长季显热和GPP的有较高的判定系数。*PAR*与GPP具有很小的判定系数，这表明该站点光照充足，植被的光合作用没有受到光照的抑制。该站点MODIS的LST产品与GPP的判定系数较小，主要是由两个方面的原因造成：(1)MODIS观测的混合像元中植被和裸土的比例随着植被的生长和凋落在变化，使得地表温度的变化趋势和GPP的变化趋势产生了不一致；(2)云和气溶胶等影响了MODIS LST反演，带来了一定误差。

本研究比较的4个模型中VPM、EC-LUE和VI模型的输入数据既包括气象观测的温度和辐射数据，又包括了通过遥感获得的植被指数数据。VPM模型和VI模型都采用了EVI来计算GPP，而EC-LUE采用的是NDVI。通过前文的分析，EVI与GPP的相关性要高于NDVI，这是EC-LUE模型精度低于这两个模型的原因之一。本研究中用于计算EC-LUE模型中水分胁迫指数的潜热和显热数据都是来自涡动相关的观测，而涡动相关存在能量不闭合的问题，其观测的显热和潜热数据有一定的误差，所以这也给EC-LUE模型带来了一定的误差。TG模型是一个完全应用遥感数据来计算GPP的光能利用率模型，它的输入包括EVI和LST。从前面的结果中可以看出，LST与GPP的相关性并不是很好，明显低于气象站观测的温度与GPP的相关性，这是导致TG模型精度较低的一个主要原因。遥感反演LST时受云、气溶胶等影响，其中包含了一定的噪声。VI和TG模型在形式上相对简单，需要的参数和输入数据相对较少，进行大尺度的GPP估算时比较容易实现，而且可以避免网格气象资料带来的不确定性。Zhao等人(2006)分别用NASA DAO、NCEP和ECMWF的气象在分析资料驱动MODIS-PSN模型来估算全球的GPP，发现其结果存在显著的差异(Zhao 等， 2006)。VPM和EC-LUE适合在有较完善的气象观测资料的区域进行模拟，具有较高的精度。

通过研究，本文得到以下结论：(1)阿柔站2009年的涡动相关观测的GPP、NEE和ER分别为：804.2 $gC/m^2/yr$、129.6 $gC/m^2/yr$和 673.6 $gC/m^2/yr$。该站点光合作用固定的碳有83.8%通过生态系统的呼吸作用释放到了大气中；(2)VPM、EC-LUE、VI和TG模型均能很好地模拟高寒草甸的GPP季节变化，全年最大判定系数为0.9571(VPM模型)，最小判定系数为0.9408(TG模型)，生长季的判定系数要均小于全年的判定系数，但是其值仍大于0.84。

参考文献(REFERENCES)

Heinsch F A, Reeves M, Votava P, Kang S, Milesi C, Zhao M S, Glassy J, Jolly W M, Loehman R, Bowker C F, Kimball J S, Nemani R R and Running S W. 2002. User's Guide GPP and NPP (MOD17A2/A3) Products NASA MODIS Land Algorithm. [2010-12-17] http://modis.gsfc.nasa.gov/

Huete A, Didan K, Miura T, Rodriguez E P, Gao X and Ferreira L G. 2002. Overview of the radiometric and biophysical performance of the MODIS vegetation indices. Remote Sensing of Environment, 83(1/2): 195–213 [DOI: 10.1016/S0034-4257(02)00096-2]

李新, 马明国, 王建, 刘强, 车涛, 胡泽勇, 肖青, 柳钦火, 苏培玺, 楚荣忠, 晋锐, 王维真, 冉有华. 2008. 黑河流域遥感—地面观测同步试验: 科学目标与试验方案. 地球科学进展, 23(9): 897–913

Li Z Q, Yu G R, Xiao X M, Li Y N, Zhao X Q, Ren C Y, Zhang L M and Fu Y L. 2007. Modeling gross primary production of alpine ecosystems in the Tibetan Plateau using MODIS images and climate data. Remote Sensing of Environment, 107(3): 510–519 [DOI: 10.1016/j.rse.2006.10.003]

Prince S D and Goward S N. 1995. Global primary production: a remote sensing approach. Journal of Biogeography, 22(4/5): 815–835 [DOI: 10.2307/2845983]

Rahman A F, Sims D A, Cordova V D and El-Masri B Z. 2005. Potential of MODIS EVI and surface temperature for directly estimating per-pixel ecosystem C fluxes. Geophysical Research Letters, 32, L19404: 1–4 [DOI: 10.1029/2005GL024127]

Richardson A D and Hollinger D Y. 2007. A method to estimate the additional uncertainty in gap-filled NEE resulting from long gaps in the CO_2 flux record. Agricultural and Forest Meteorology, 147(3/4): 199–208 [DOI: 10.1016/j.agrformet.2007.06.004]

Running S W, Thornton P E, Nemani R and Glassy J M. 2000. Global terrestrial gross and net primary productivity from the earth observing system // Sala O E, Jackson R B, Mooney H A and Howarth R W, eds. Methods in Ecosystem Science. New York: Springer-Verlag: 44–57

Sims D A, Rahman A F, Cordova V D, El-Masri B Z, Baldocchi D D, Bolstad P V, Flanagan L B, Goldstein A H, Hollinger D Y, Misson L, Monson R K, Oechel W C, Schmid H P, Wofsy S C and Xu L K. 2008. A new model of gross primary productivity for North American ecosystems based solely on the enhanced vegetation index and land surface temperature from MODIS. Remote Sensing of Environment, 112(4): 1633–1646 [DOI: 10.1016/j.rse.2007.08.004]

Veroustraete F, Sabbe H and Eerens H. 2002. Estimation of carbon mass fluxes over Europe using the C-Fix model and Euroflux data. Remote Sensing of Environment, 83(3): 376–399 [DOI: 10.1016/S0034–4257(02)00043–3]

Wang X F, Ma M G, Huang G H, Veroustraete F, Zhang Z H, Song Y and Tan J L. 2011. Vegetation primary production estimation at maize and alpine meadow over the Heihe River Basin, China. International Journal of Applied Earth Observation and Geoinformation, (In press) [DOI: 10.1016/j.jag.2011.09.009]

Wang Z, Xiao X M and Yan X D. 2010. Modeling gross primary production of maize cropland and degraded grassland in northeastern China. Agricultural and Forest Meteorology, 150(9): 1160–1167 [DOI: 10.1016/j.agrformet.2010.04.015]

Wohlfahrt G, Bahn M, Haslwanter A, Newesely C and Cernusca A. 2005. Estimation of daytime ecosystem respiration to determine gross primary production of a mountain meadow. Agricultural and Forest Meteorology, 130(1/2): 13–25 [DOI: 10.1016/j.agrformet.2005.02.001]

Wu C Y, Han X Z, Ni J S, Niu Z and Huang W J. 2010. Estimation of gross primary production in wheat from in situ measurements. International Journal of Applied Earth Observation and Geoinformation, 12(3): 183–189 [DOI: 10.1016/j.jag.2010.02.006]

吴力博, 古松, 赵亮, 徐世晓, 周华坤, 冯超, 徐维新, 李英年, 赵新全, 唐艳鸿. 2010. 三江源地区人工草地的生态系统CO_2净交换、总初级生产力及其影响因子. 植物生态学报, 34(7): 770–780

伍维华. 2002. 植物生理学. 北京: 科学出版社: 172–173

Wu W X, Wang S Q, Xiao X M, Yu G R, Fu Y L and Hao Y B. 2008. Modeling gross primary production of a temperate grassland ecosystem in Inner Mongolia, China, using MODIS imagery and climate data. Science in China Series D: Earth Sciences, 51(10): 1501–1512

Xiao X M, Hollinger D, Aber J, Goltz M, Davidson E A, Zhang Q Y and Moore B III. 2004. Satellite-based modeling of gross primary production in an evergreen needleleaf forest. Remote Sensing of Environment, 89(4): 519–534 [DOI: 10.1016/j.rse.2003.11.008]

Xiao X M, Zhang Q Y, Hollinger D, Aber J and Moore B. 2005. Modeling gross primary production of an evergreen needleleaf forest using MODIS and climate data. Ecological Applications, 15(3): 954–969 [DOI: 10.1890/04-0470]

Yan H M, Fu Y L, Xiao X M, Huang H Q, He H L and Ediger L. 2009. Modeling gross primary productivity for winter wheat-maize double cropping system using MODIS time series and CO_2 eddy flux tower data. Agriculture, Ecosystems and Environment, 129(4): 391–400 [DOI: 10.1016/j.agee.2008.10.017]

Yuan W P, Liu S G, Zhou G H, Zhou G Y, Tieszen L L, Baldocchi D, Bernhofer C, Gholz H, Goldstein A H, Goulden M L, Hollinger D Y, Hu Y M, Law B E, Stoy P C, Vesala T and Wofsy S C. 2007. Deriving a light use efficiency model from eddy covariance flux data for predicting daily gross primary production across biomes. Agricultural and Forest Meteorology, 143(3/4): 189–207 [DOI: 10.1016/j.agrformet.2006.12.001]

Yuan W P, Liu S G, Yu G R, Bonnefond J M, Chen J Q, Davis K, Desai A R, Goldstein A H, Gianelle D, Rossi F, Suyker A E and Verma S B. 2010. Global estimates of evapotranspiration and gross primary production based on MODIS and global meteorology data. Remote Sensing of Environment, 114(7): 1416–1431 [DOI: 10.1016/j.rse.2010.01.022]

张智慧, 王维真, 马明国, 徐自为, 吴月茹, 黄广辉, 谭俊磊. 2010. 黑河综合遥感联合试验涡动相关通量数据处理及产品分析. 遥感技术与应用, 25(6): 788–796

Zhao M S, Running S W and Nemani R R. 2006. Sensitivity of Moderate Resolution Imaging Spectroradiometer (MODIS) terrestrial primary production to the accuracy of meteorological reanalyses. Journal of Geophysical Research, 111: G01002 [DOI: 10.1029/2004JG000004]

Zhu Z L, Sun X M, Wen X F, Zhou Y L, Tian J and Yuan G F. 2006. Study on the processing method of nighttime CO_2 eddy covariance flux data in ChinaFLUX. Science in China Series D: Earth Sciences. 49(Supp. II): 36–46 [DOI: 10.1007/s11430-006-8036-5]